Thermoresistance of p-type 4H-SiC integrated MEMS devices for high-temperature sensing[†]

Toan Dinh[*‡], *Tuan-Khoa Nguyen, Hoang-Phuong Phan, Quan Nguyen, Jisheng Han, Sima Dimitrijev, Nam-Trung Nguyen, and Dzung Viet Dao*

[†]   *Dr. T. Dinh, Mr. T.-K. Nguyen, Dr. H.-P. Phan,   A/Prof. Dr. Jisheng Han, Prof. Dr. Sima Dimitrijev, Prof. Dr.   Nam-Trung Nguyen and A/Prof. Dr. Dzung Viet Dao*
Queensland Micro and Nanotechnology Centre
Griffith University, West Creek Road, Nathan, Qld 4111, Australia
[*] *E-mail: toan.dinh@griffithuni.edu.au*

Abstract

There is an increasing demand for the development and integration of multifunctional sensing modules into power electronic devices that can operate in high temperature environments. Here, we demonstrate the tunable thermoresistance of p-type 4H-SiC for a wide temperature range from the room temperature to above 800 K with integrated flow sensing functionality into a single power electronic chip. The electrical resistance of p-type 4H-SiC was found to exponentially decrease with increasing temperature to a threshold temperature of 536 K. The temperature coefficient of resistance (TCR) showed a large and negative value from -2,100 to -7,600 ppm/K, corresponding to a thermal index of 625 K. From the threshold temperature of 536 K to 846 K, the electrical resistance showed excellent linearity with a positive TCR value of 900 ppm/K. We successfully demonstrated the integration of p-4H-SiC flow sensing functionality with a high sensitivity of 1.035 $\mu A(m/s)^{-0.5}/mW$. These insights in the electrical transport of p-4H-SiC will aid to improve the performance of p-4H-SiC integrated temperature and flow sensing systems, as well as the design consideration and integration of thermal sensors into 4H-SiC power electronic systems operating at high temperatures of up to 846 K.

1. Introduction

Due to the difficulty of locating sensing components in harsh environments, the current sensing devices have replied on indirect measurement technologies which are complex and expensive. Consequently, sensors and electronics that can operate in hostile conditions have been of high interest and great demand for a wide range of applications, including deep space exploration, combustion monitoring, and examination of hypersonic aircrafts [1,2]. However, electronic sensing systems have deployed conventional sensing materials such as metal and silicon, which cannot operate reliably in high-temperature and high corrosive conditions. Therefore, there have been new requirements for sensing technologies working beyond the capability of silicon which typically functions as a sensing material for a temperature less than 200°C.

SiC has attracted a great deal of attention for sensing applications in harsh environments, owing to its superior mechanical/electrical properties [3-6]. As such, the high breakdown field of SiC (4×10^6 V/cm) has been employed to develop high power electronic devices [7]. Moreover, SiC has a higher energy gap as compared to its counterpart silicon (e.g. 1.1 eV for Si, 2.3 eV for 3C-SiC and 3.2 eV for 4H-SiC) which leads to a better thermal stability of SiC at high temperatures [8,9]. The high thermal conductivity of 5 Wcm^{-1}K^{-1} and high melting point of 2830°C make SiC a potential candidate for electronics operating at high temperatures [2,3,8,9]. As SiC sensing devices can be mass-produced with conventional mature micro/nano machining technologies including MEMS (Micro ElectroMechanical Systems) and IC (Integrated Circuit), the cost of such devices can be significantly reduced.

Employing MEMS and IC technologies, several temperature sensing devices have been successfully demonstrated for a working temperature of up to 300°C, including Schottky diodes and p-n junctions [10-18]. However, the performance of these devices significantly declines at high temperatures. For example, 4H-SiC Schottky junction temperature sensors have been demonstrated with a sensitivity of 2.66 mV/K and linearity up to 573 K [18]. The significant decrease of the Schottky barrier at elevated temperatures has limited applications

of such sensing devices which are only capable of operating in the low temperature range. In addition, SiC power devices, including metal-oxide-semiconductor field-effect transistors (MOSFETs) [13], have been commercialised for high-voltage (e.g. up to 1.7 kV) applications. However, these devices can only work reliably for a temperature range of up to 573 K (300°C).

The limitation of the working temperature of SiC power devices is not only deduced from the packaging issues but also the difficulty in integrated on-chip temperature sensing modules. The temperature sensing components integrated in a single chip with capability of working at high temperatures above 500°C will be highly favorable to a wide range of high power devices and industrial applications. The capability of locating the sensing modules on the hot spot areas will also enable the accurate and real-time measurement of the electronic systems in high temperature environments. More importantly, multiple integrated sensing devices including temperature and flow sensing functionalities are beneficial to maintain the safety and efficiency of electronic systems working in harsh environments. To date, due to a number of great challenges, very limited work has demonstrated the integrated 4H-SiC temperature sensing devices at high temperatures. The challenges include, but are not limited to, the accessibility to high quality p-type 4H-SiC materials, and the formation of Ohmic contact to p-type 4H-SiC, especially at high temperatures. These impede the development of 4H-SiC thermal sensing systems and their integration into a single 4H-SiC power electronic chip. Understanding of thermally-mediated physical transport of carriers at high temperatures could boost the development and integration of 4H-SiC multifunctional sensing modules into the 4H-SiC electronic system operating in harsh environments.

In the present work, we demonstrate the high-performance 4H-SiC temperature sensing devices for temperatures above 300°C, with integrated flow sensing functionality. The simple fabrication strategy to integrate 4H-SiC temperature and flow sensing modules in a single chip using MEMS technologies are also presented. The results showed the tunability of the

electrical transport properties of p-type 4H-SiC for a wide temperature range of room temperature to above 846 K (~570°C). We found a threshold temperature that can change the temperature coefficient of resistance (TCR) of 4H-SiC from negative to positive. This threshold temperature contributes to a thermal energy level where the number of inonized carriers is saturated, while the effect of carrier scattering is dominant at higher temperatures. This leads to the high linearity of the sensor characteristic at high temperatures (above 300°C to 570°C). In addition, the integrated flow sensing module was successfully demonstrated with a high sensitivity of 1.035 µA(m/s)$^{-0.5}$/mW. Our work demonstrates the feasibility of the p-type 4H-SiC sensing technology working in high-temperature environments and operating beyond the capability of conventional materials such as silicon. Compared to 3C-SiC on glass [14] and graphite on paper [19], 4H-SiC can work at much higher temperatures. As such, while graphite and 3C-SiC can operate at a temperature of below 150°C, and 300°C, respectively, 4H-SiC can serve as a sensitive temperature sensing material up to 570°C. In fact, the working temperature of both graphite and 3C-SiC limits by the devices themselves, while the highest operating temperature of 4H-SiC is limited by the testing facility. Our findings not only provided the insights into the thermally-mediated physical transport of charge carriers in p-4H-SiC at high temperatures but also successfully demonstrated the high potential of integrating temperature and flow sensing modules into a single 4H-SiC platform that could be utilized for fully integrated 4H-SiC power electronic systems.

2. Experimental

2.1 Fabrication of thermoresistors and flow sensors

The SiC substrate was a 4H-SiC wafer, purchased from Cree^{TM}. The functional p-type layer, with a doping concentration of 10^{18} cm^{-3}, resistivity of 0.91 Ωcm and thickness of 1 µm, was epitaxially grown on 1-µm thick n-type layer (Figure 1a). The substrate was highly resistive intrinsic 4H-SiC with a thickness of 300 µm. We employed a conventional MEMS (Micro ElectroMechanical System) process to form p-type 4H-SiC (p-4H-SiC) thermoresistors as

4

shown in Figure 1 (b) to (f). First, a 4 µm-thick photoresist (PR) was spin-coated on the p-type layer (Figure 1b), followed by a photolithography step to pattern the thermoresistors (Figure 1c). The p-type SiC was then etched using a Inductive Coupled Plasma etching at an etching rate of approximately 100 nm/min (Figure 1d). In the next step, titanium (Ti) and aluminum (Al) layers were coated using a sputtering method and then patterned to form electrodes (Figure 1 e and f). Finally, an annealing process was conducted in air, with a temperature ramp-up rate of $100^{o}C$ /min and holding time of 2 min at $1000^{o}C$. This process formed Ohmic contacts to p-4H-SiC.

(a) p-4H-SiC wafer   (b) Coating photoresist (PR)   (c) Patterning PR

(d) Etching SiC   (e) Deposition & etching of Ti/Al
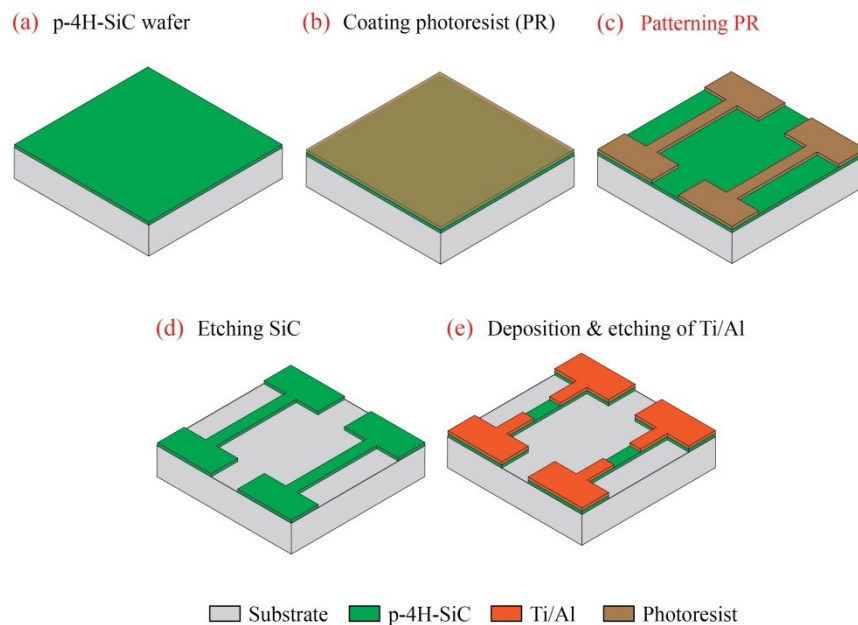
☐ Substrate ☐ p-4H-SiC ☐ Ti/Al ☐ Photoresist

Figure 1. MEMS process for fabrication of 4H-SiC thermoresistors.

2.2 Experimental setup

To investigate the thermoresistive characteristics of p-4H-SiC at high temperatures, we employed a high temperature Linkam stage (Figure S1, Supporting Information). The p-4H-SiC device was clamped and wirebonding was used to electrically connect the Ti/Al electrodes to the copper pads. The current-voltage (I-V) measurements were performed at different applied temperatures, using a source meter (Keithley 2450). The measurement was conducted in an enclosed chamber to reduce the thermal noise from the environment.

In addition, we used a flow setup (Figure S2, Supporting Information) for the characterization of the p-4H-SiC flow sensors. For the demonstration of flow sensing, a pipe with a diameter

of D=5 cm and a length of 1.5 m was used as a flow channel. Air flow with a range of 1 to 10 m/s was generated from an air blower and the flow velocities were measured using a reference flow sensor (Testo 405i, accuracy/resolution 0.1 m/s and max air velocity of 30 m/s). The flow condition was determined based on the calculated Reynold number as $R_e = \rho v D/\mu$, where ρ=1.1839 kg/m^3 and μ=1.846×10^{-5} m^2/s are the density and dynamic viscosity of air, respectively. Therefore, the Reynolds number was estimated ranging from 3200 to 32000, indicating a turbulent flow regime (R_e>2600).

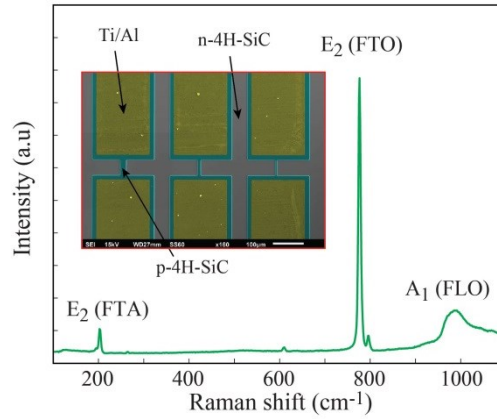## 3. Results and discussion

3.1. 4H-SiC material

Figure 2. Raman spectrum of 4H-SiC. The inset shows the as-fabricated 4H-SiC thermoresistors.

Figure 2 shows the Raman spectrum of the 4H-SiC samples at the room temperature (297 K). There are three dominant peaks at the wavenumbers of 204, 776, 965 cm^{-1}, corresponding to the folded transverse acoustic (FTA), folded transverse optic E$_2$ (FTO), and longitudinal optical (FLO) modes, respectively. This result indicates that the 4H-SiC material was between the Ti/Al coatings. The inset in Figure 2 illustrates the as-fabricated p-type 4H-SiC thermoresistors. We employed a Dektak surface profiler to confirm the etching depth of 1.3 µm to the 4H-SiC substrate.

3.2. Tunable thermoresistance

To characterize the thermoresistive effect in a single p-4H-SiC layer, we first confirmed the Ohmic contact of the thermoresistors to their electrodes by measuring the relevant current-

voltage (I-V) characteristics. Figure 3 shows the I-V measurement results, indicating a linear characteristic of the as-fabricated devices at different temperatures. The linear characteristics were observed at all temperatures from 297 to 846 K, indicating the excellent Ohmic contact at elevated temperatures. The I-V curves go through the origin of the coordinates axis, indicating that the thermoelectric effect has no influence on the electrical measurement. The leakage current to the substrate was also measured over a wide temperature range and confirmed as negligible for the thermoresistive measurements (not shown here). Figure 3a shows the change of I-V characteristics with a temperature range from the room temperature (297 K) to above 536 K. Figure 3b shows a zoom-in plot of the current change within this temperature range. Evidently, at a constant applied voltage, the measured current increased with increasing temperature, indicating that the conduction of p-4H-SiC is thermally activated in the temperature range from the room temperature to above 536 K (Figure 3a). The increase of the current I is from 27.8 to 61.9 µA (2.2 times) at an applied voltage of 1.8 V when the temperature increases from 297 to 536 K. However, at temperatures above 536 K, the I-V characteristics show the inverse effect with changing temperature (Figure 3c). As such, the zoom-in graph in Figure 3d shows a decrease of the measured current with increasing temperature. The measured current decreases from 61.9 to 46.2 µA (1.34 times) when the temperature increases from 536 to 846 K. This thermally-mediated inverse effect suggests a change of charge transport mechanism with increasing thermal energy. This current change corresponds to a variation of the electrical resistance R of p-4H-SiC, which is defined by the Ohm's law: $R=V/I$. The resistance change $\Delta R/R$ is calculated as $\Delta R/R=(R-R_o)/R_o$, where R and R_o are the resistance of p-4H-SiC at temperature T and reference temperature T_o, respectively. Figure 4a shows reductions of p-4H-SiC electrical resistance with increasing temperature to 536 K. The resistance decreased more than 55% when the temperature reached 536 K. The corresponding to a temperature coefficient of resistance (TCR) of p-4H-SiC ($TCR= \Delta R/R \times 1/ \Delta T$) ranges from -2,100 ppm/K to -7,600 ppm/K for the temperature range of 297 to 536 K.

7

The *TCR* is comparable with and even better than the temperature coefficient of various conventional metals and highly doped silicon used for MEMS thermal sensors [3,20], such as platinum (*TCR*~3,920 ppm/K). The results indicate the high potential of p-4H-SiC for highly sensitive and robust temperature sensors at temperatures below 536 K. At temperatures above 536 K, the TCR changed to be positive with its maximum value of 900 ppm/K at 846 K. More interestingly, the p-type temperature sensing device showed its excellent linearity for the high temperature regime. This characteristic is of high interest for electronic devices working at high temperatures in terms of the simplicity in design and implementation of circuitry. To understand the electrical transport properties, the following section will discuss the conduction mechanism of p-4H-SiC at high temperatures.
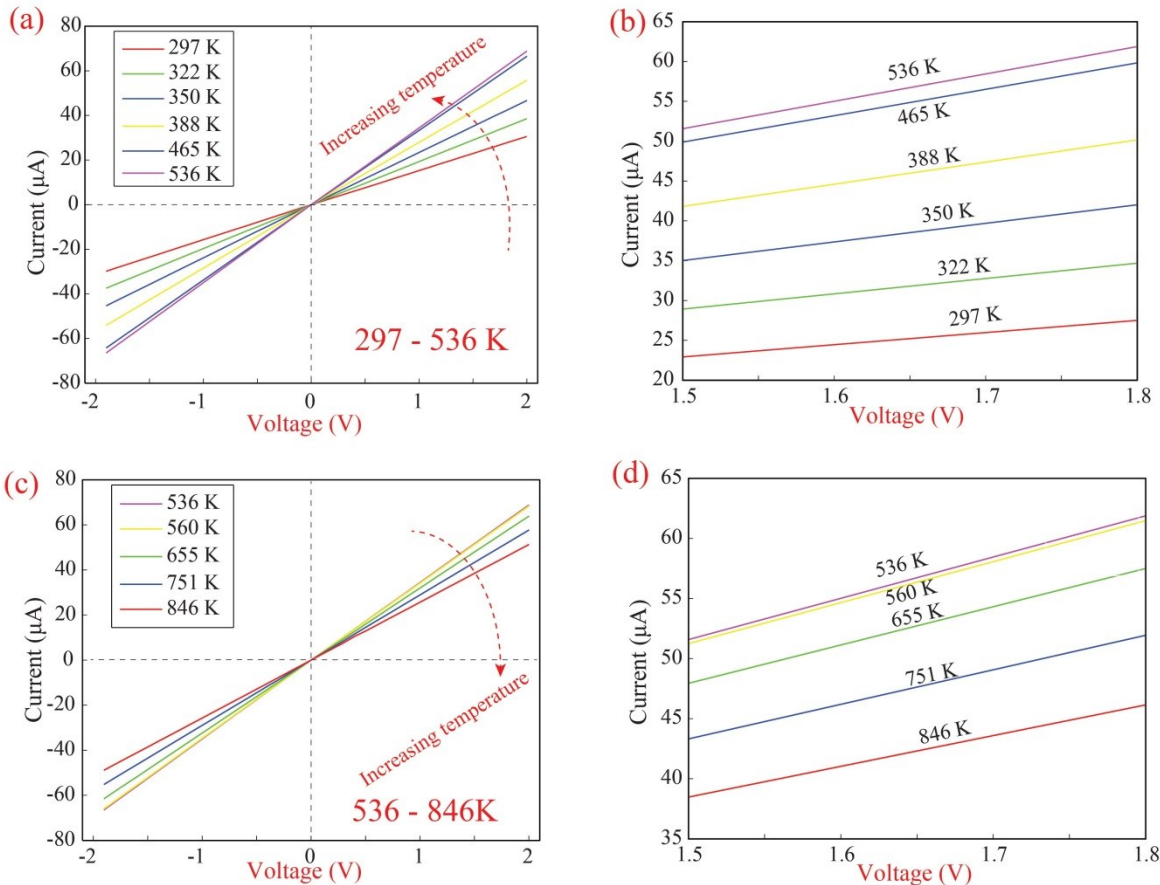

Figure 3. Temperature effect on the electrical properties of p-type 4H-SiC. (a,b) Current-voltage (I-V) characteristics of the p-4H-SiC thermoresistors at temperatures up to 536 K. (c,d) I-V characteristics of the p-4H-SiC thermoresistors from 536 to 846 K.

The thermally activated conduction of p-4H-SiC with increasing thermal energy is attributed to the increase in the concentration of hole and decrease of its mobility, where the former is dominant at temperatures below 536 K, leading to an increase of conductivity or decrease of resistivity [21,25]. As temperature increase from 297 to 536 K, more acceptors in p-4H-SiC become ionised and donate their holes to the valence band. The thermal generation of carriers from the valence band to the conduction band is negligible because of high energy gap of 4H-SiC (3.2 eV). The hole concentration p can be expressed by the following relationship:

$$\ln(p) \sim \alpha \ln(T) - \frac{E_a}{kT} \tag{1}$$

where E_a is the activation energy and $k=1.38 \times 10^{-23}$ $m^2 kgs^{-2}K^{-1}$ is the Boltzmann constant. The decrease of hole mobility with increasing temperature is attributed to the acoustic phonon scattering with the temperature dependence of mobility µ on temperature described in the following form [24-27] $ln(\mu)=-\beta\, lnT$, where β is a constant. Therefore, the conductivity (σ) of p-4H-SiC material in the temperature range of 297 to 536 K can be described in the following way:

$$\ln(\sigma) \sim \ln(n) + \ln(\mu) \sim (\alpha - \beta)\ln(T) - \frac{E_a}{kT} \tag{2}$$

For temperature sensing, the p-4H-SiC thermoresistors can function as a resistive temperature detector where its electrical resistance change can be simply described as:

$$\ln\left(\frac{R}{R_o}\right) \sim A + \frac{B}{T} \tag{3}$$

where A is a constant and $B = E_a/k$ is the thermal index of p-4H-SiC. To estimate the B value, we employed the Arrhenius plot to find the thermal index threshold in the temperature range from 297 K to 536 K (Figure 4b). The thermal index was found to be 625 K for the low temperature range (below 536 K). The thermal index of p-4H-SiC is comparable with that of other temperature sensors reported in the literature [14,30,31]. Therefore, p-4H-SiC thermoresistors are suitable for the highly accurate measurements of temperature.
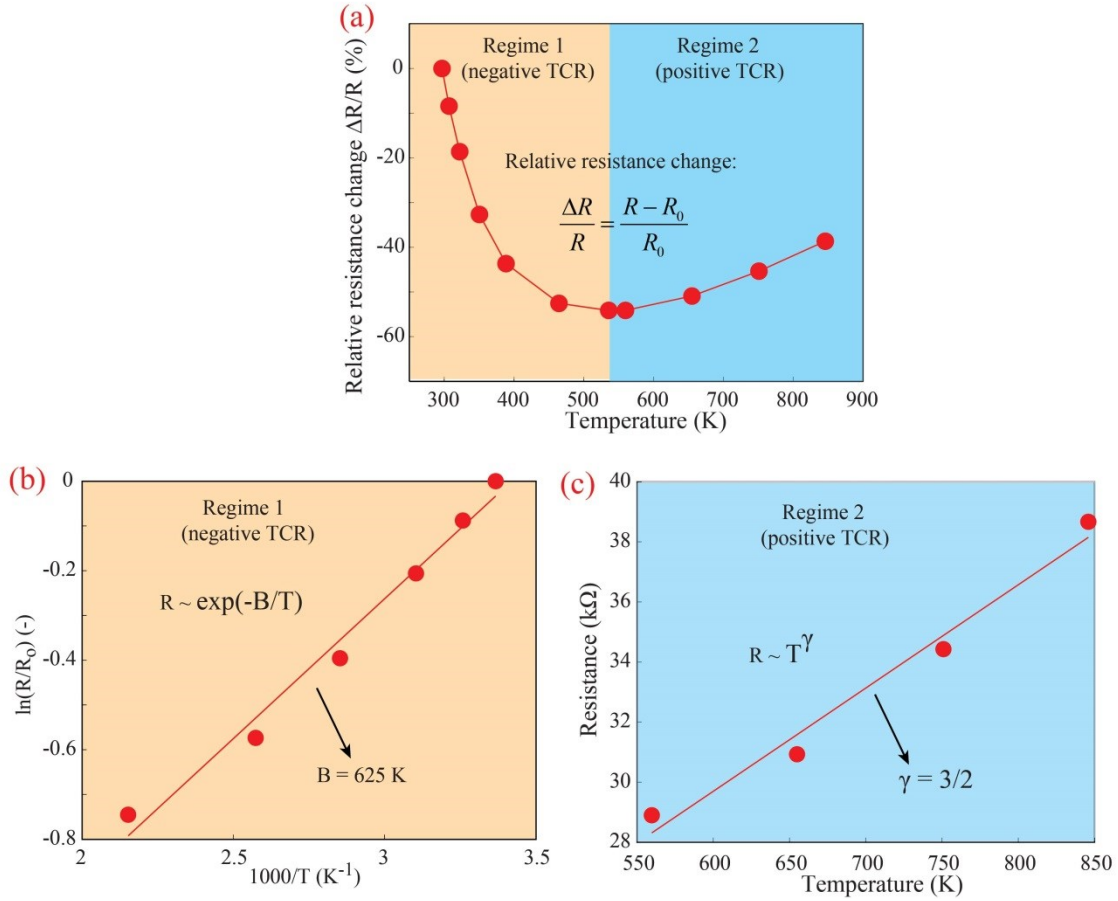
Figure 4. Tunable electrical transport in p-4H-SiC. (a) Electrical resistance change with temperature. (b) Arrhenius plot of p-4H-SiC thermoresistance for the temperature range from 297 to 536 K. (c) Plot of thermoresistance in p-4H-SiC for temperature range of 536 to 846 K, showing a relationship of $R \sim T^{\gamma}$ with $\gamma = 3/2$.

In a higher temperature range of 536 to 846 K, all acceptors have been ionised and donated to the valence band, leading to a constant concentration of holes in the valence band. However, the hole mobility still decreases with increasing temperature, leading to an increase of the electrical resistance of p-4H-SiC in this temperature range. From Equation 2, the resistance dependence on temperature can be presented in the form $R \sim T^{\gamma}$, where $\gamma = 3/2$ (Figure 4c).

3.3. Joule heating effect and flow sensing characteristics

To integrate the flow sensing functionality into the temperature sensing device, we investigated the Joule heating effect of the device, in which the temperature of the p-4H-SiC material is raised to a steady state under a constant applied voltage/current/power. The steady state is maintained by the law of energy balance between Joule heating and convective/conductive cooling. For simplicity of testing the flow sensing functionality, we

10

used a 1 μm-thick 500×3000 μm^2 p-4H-SiC thermoresistor. At temperatures lower than 536 K, the electrical resistance of p-4H-SiC decreases with increasing temperature owing to its negative TCR. Under a low applied power/voltage (less than 10 V), the I-V characteristic is linear (Figure 5a). This I-V becomes non-linear at higher applied voltages. At an applied power above 50 mW, the resistance of the p-4H-SiC thermoresistor decreases, leading to a non-linear I-V characteristic. Figure 5b shows the dependence of electrical resistance on the dissipated power. It is evident that the resistance decreases with increasing power.
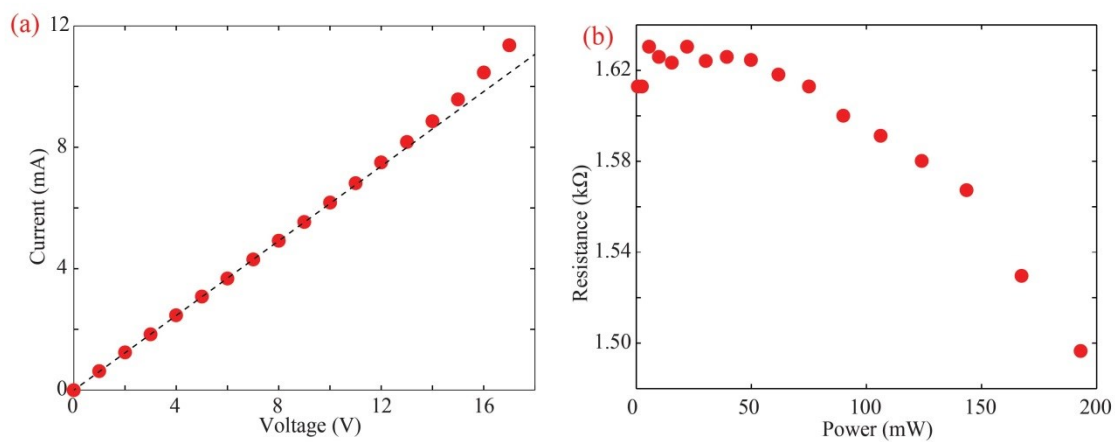

Figure 5. Joule heating effect in p-4H-SiC. (a) Non-linear I-V characteristics of p-4H-SiC film. (b) The dependence of p-4H-SiC electrical resistance on dissipated electric power.

When a flow is applied, the temperature of the p-4H-SiC film decreases due to forced cooling effect, leading to the increase in the electrical resistance of the film. Under a constant applied voltage, the measured current will decrease owing to the negative temperature coefficient of resistance of the p-4H-SiC film. Figure 6 shows the real-time response of the p-4H-SiC flow sensing module to different air flow velocities. The measured current decreases gradually when the input flow is applied (ON) for 30 s, then it increases to the initial value when the flow velocity turns to zero within 90 s. Under a supply voltage of 18 V, the measured current change varied from 0.4 mA to 0.8 mA when air velocities increased from 2.8 m/s to 8.4 m/s, respectively. This increase indicates the more effective cooling effect on the p-4H-SiC flow sensing device under higher applied input air speeds. Under a constant voltage mode, the

relationship between the differential output current and the applied velocity is empirically expressed by King's law [19,32]:
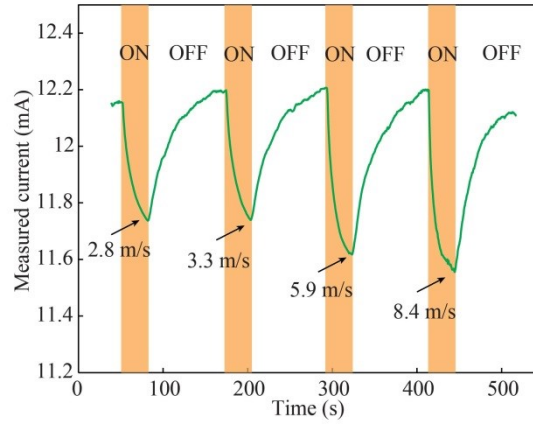

Figure 6. The response of p-4H-SiC thermal flow sensing device to different applied air velocities.

$$\Delta I = a + b\upsilon^n \tag{4}$$

where ΔI is the change of measured current and υ is the air velocity. Figure 7 shows the change of the measured current under various input air velocities. It is evident that the measured current is more pronounced with a higher applied power/voltage or under higher input air speeds. Table 1 (Supporting Information) summarizes the performance of the p-4H-SiC flow sensing module in comparison with the literature. The sensitivity of the flow sensing module is defined as $S = \dfrac{\Delta I}{I} \dfrac{1}{\upsilon^{0.5}} \dfrac{1}{P}$, where P is the power consumption of the device. The sensitivity of the flow sensing module was estimated to be 1.035 $\mu A(m/s)^{-1/2}/mW$, which is better than that of other MEMS flow sensors [31,33-37]. This indicates that the flow sensing module was successfully integrated in to the system with high sensitivity. The capability of the temperature sensing module operating at high temperatures and the successful integration of the flow sensing module have demonstrated the strong feasibility of using p-type 4H-SiC sensing technology for integrated multifunctional sensing modules operating in high-temperature and harsh environments.
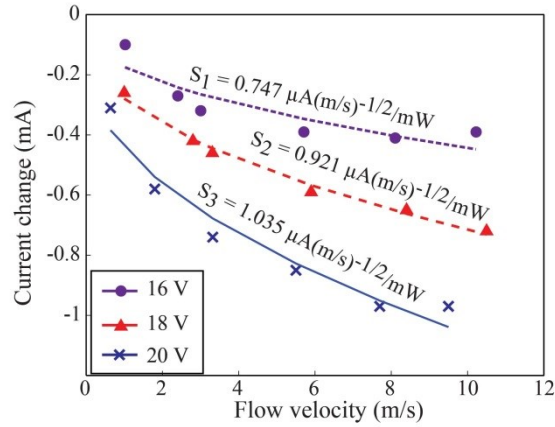
Figure 7. Measured current under different applied voltage/power and different input air velocities.

4. Conclusion

In the conclusion, this work has successfully demonstrated p-type 4H-SiC temperature and flow integrated sensing devices capable of operating at high temperature up to 846 K. The tunability of the electrical transport in p-type 4H-SiC was observed. The p-type 4H-SiC showed the excellent linearity and robustness at high temperatures (above 536 K to 846 K) with a temperature coefficient of resistance of 900 ppm/K, as well as a high temperature sensitivity of up to 7,600 ppm/K at a lower temperature range (less than 536 K). The Joule heating effect in p-4H-SiC was employed to develop the flow sensing module with a high sensitivity of 1.035 $\mu A(m/s)^{-0.5}$/mW. The successful investigation of the thermoresistance in p-4H-SiC with integrated flow sensing functionality, demonstrates the high potential of p-4H-SiC for robust sensing systems capable of working in high temperature environments. The insights into the high-temperature sensing mechanism of p-type 4H-SiC will strongly support for the design and improvement of the sensing systems at high temperatures, which operate beyond the capability of conventional sensing materials such as silicon.

Reference

 [1] M. R. Werner and W. R. Fahrner, *IEEE Transactions on Industrial Electronics*, **2001**, 48, 249-257.

[2] M. Mehregany and C. A. Zorman, Thin solid films, **1999**, 355, 518-524.

[3] T. Dinh, H.-P. Phan, A. Qamar, P. Woodfield, N.-T. Nguyen and D. V. Dao, *Journal of Microelectromechanical Systems*, **2017**.

[4] N. Wright and A. Horsfall, *Journal of Physics D: Applied Physics*, **2007**, 40, 6345.

[5] A. Qamar, T. Dinh, M. Jafari, A. Iacopi, S. Dimitrijev and D. V. Dao, *Materials Letters*, **2018**, 213, 11-14.

[6] H.-P. Phan, T. Dinh, T. Kozeki, T.-K. Nguyen, A. Qamar, T. Namazu, N.-T. Nguyen, D. V. Dao, *Applied Physics Letters 2016, 109, 123502.*

[7] C. E. Weitzel, J. W. Palmour, C. H. Carter, K. Moore, K. Nordquist, S. Allen, C. Thero and M. Bhatnagar, *IEEE Transactions on Electron Devices*, **1996**, 43, 1732-1741.

[8] J. Casady and R.W. Johnson, *Solid-State Electronics*, **1996**, 39, 1409-1422.

[9] N. Zhang, C.-M. Lin, D. G. Senesky and A. P. Pisano, *Applied Physics Letters*, **2014**, 104, 073504.

[10] D. Peters, R. Schrner, K.-H. Hlzlein and P. Friedrichs, *Applied physics letters*, **1997**, 71, 2996-2997.

[11] A. Kadavelugu, V. Baliga, S. Bhattacharya, M. Das and A. Agarwal, **2011.**

[12] W.-C. Lien, D.-S. Tsai, D.-H. Lien, D. G. Senesky, J.-H. He and A. P. Pisano, *IEEE Electron Device Letters*, **2012**, 33, 1586-1588.

[13] M. Berthou, P. Godignon and J. Milln*, IEEE Transactions on Power Electronics*, **2014**, 29, 4970-4977.

[14] T. Dinh, H.-P. Phan, T. Kozeki, A. Qamar, T. Namazu, N.-T. Nguyen and D. V. Dao, *RSC Advances*, **2015**, 5, 106083-106086.

[15] S. Rao, G. Pangallo and F. G. Della Corte, *IEEE Electron Device Letters*, **2015**, 36, 1205-1208.

[16] H.-P. Phan, A. Qamar, D. V. Dao, T. Dinh, L. Wang, J. Han, P. Tanner, S. Dimitrijev, N.-T. Nguyen, *RSC Advances* **2015**, 5, 56377.

[17] S. Rao, G. Pangallo, F. Pezzimenti and F. G. Della Corte, *IEEE Electron Device Letters*, **2015**, 36, 720-722.

[18] S. Rao, G. Pangallo and F. G. Della Corte, *IEEE Transactions on Electron Devices*, **2016**, 63, 414-418.

[19] T. Dinh, H.-P. Phan, D. V. Dao, P. Woodfield, A. Qamar and N.-T. Nguyen, *Journal of Materials Chemistry C,* **2015**, 3, 8776-8779.

[20] F. Warkusz, *Journal of Physics D: Applied Physics*, **1978**, 11, 689.

[21] W. Gtz, A. Schner, G. Pensl, W. Suttrop, W. Choyke, R. Stein and S. Leibenzeder, *Journal of applied physics*, **1993**, 73, 3332-3338.

[22] J. Pernot, S. Contreras, J. Camassel, J. Robert, W. Zawadzki, E. Neyret and L. Di Cioccio, *Applied Physics Letters*, **2000**, 77, 4359-4361.

[23] H. Matsuura, M. Komeda, S. Kagamihara, H. Iwata, R. Ishihara, T. Hatakeyama, T. Watanabe, K. Kojima, T. Shinohe and K. Arai, *Journal of Applied Physics*, **2004**, 96, 2708-2715.

[24] H. Iwata and K. M. Itoh, *Journal of Applied Physics*, **2001**, 89, 6228-6234.

[25] J. Pernot, W. Zawadzki, S. Contreras, J. Robert, E. Neyret and L. Di Cioccio, *Journal of Applied Physics*, **2001**, 90, 1869-1878.

[26] D. Barrett and R. Campbell, *Journal of Applied Physics*, **1967**, 38, 53-55.

[27] T. Dinh, H.-P. Phan, T. Kozeki, A. Qamar, T. Fujii, T. Namazu, N.-T. Nguyen, D. V. Dao, *Materials Letters* **2016**, 177, 80.

[28] M. Roschke and F. Schwierz, *IEEE Transactions on Electron Devices*, **2001**, 48, 1442-1447.

[29] M. Yamanaka, H. Daimon, E. Sakuma, S. Misawa and S. Yoshida, *Journal of applied physics*, **1987**, 61, 599-603.

[30] A. Feteira, *Journal of the American Ceramic Society*, **2009**, 92, 967-983.

[31] T. Dinh, H.-P. Phan, T.-K. Nguyen, A. Qamar, A. R. M. Foisal, T. N. Viet, C.-D. Tran, Y. Zhu, N.-T. Nguyen and D. V. Dao, *Journal of Materials Chemistry C*, **2016**, 4, 10061-10068.

[32] J. T. Kuo, L. Yu and E. Meng, *Micromachines*, **2012**, 3, 550-573.

 [33] S.-T. Hung, S.-C. Wong and W. Fang, *Sensors and Actuators A: Physical*, **2000**, 84, 70-75.

[34] G. Kaltsas, P. Katsikogiannis, P. Asimakopoulos and A. Nassiopoulou, *Measurement Science and Technology*, **2007**, 18, 3617.

[35] F. Mailly, A. Giani, R. Bonnot, P. Temple-Boyer, F. Pascal- Delannoy, A. Foucaran and A. Boyer, *Sensors and Actuators A: Physical*, **2001**, 94, 32-38.

[36] G. Kaltsas, A. A. Nassiopoulos and A. G. Nassiopoulou, *IEEE Sensors Journal*, **2002**, 2, 463-475.

[37] F. Zhao, W. Du and C.-F. Huang, *Microelectronic Engineering*, **2014**, 129, 53-57.